Thermoelectric properties of n-type cobalt doped chalcopyrite Cu1–xCoxFeS2 and p-type eskebornite CuFeSe2

David Berthebaud, O.I. Lebedev, A. Maignan

Available online at www.sciencedirect.com

ScienceDirect

Journal of Materiomics 1 (2015) 68–74

www.ceramsoc.com/en/

www.journals.elsevier.com/journal-of-materiomics/

Thermoelectric properties of *n*-type cobalt doped chalcopyrite $Cu_{1-x}Co_xFeS_2$ and *p*-type eskebornite $CuFeSe_2$

D. Berthebaud, O.I. Lebedev, A. Maignan*

Laboratoire CRISMAT, UMR 6508 CNRS/ENSICAEN, 6 bd du Maréchal Juin, F-14050 CAEN Cedex 4, France

Received 24 December 2014; revised 8 January 2015; accepted 30 January 2015
Available online 1 April 2015

Abstract

Chalcopyrite $CuFeS_2$ has been recently suggested as a promising thermoelectric material. In the present paper, the transport properties – electrical resistivity ρ and Seebeck coefficient S – of the *n*-type $CuFeS_2$ chalcopyrite and the *p*-type $CuFeSe_2$ eskebornite have been measured. Very different groundstates are evidenced with a semimetallic behavior concomitant to a metal-like S(T) curve for $CuFeSe_2$ whereas $CuFeS_2$ is a semiconductor with much larger |S| values. For that reason, charge creation by Co^{2+} for Cu^{+} substitution in $CuFeS_2$ has been performed. The veracity of the Co for Cu substitution for $x \leq 0.10$ in $Cu_{1-x}Co_xFeS_2$ chalcopyrite has been confirmed by EDS analyses, coupled to electron diffraction, with a transmission electron microscope. Also, this study demonstrates the existence of twinning domains. The compounds corresponding to the best compositions in terms of power factor have been densified by Spark Plasma Sintering for thermal conductivity measurements. A maximum *ZT* value up to 0.22 at 675 K for $Cu_{0.96}Co_{0.04}FeS_2$ has been obtained.

Keywords: Chalcogenides; Thermoelectric material; Thermal conductivity

1. Introduction

In the past few years, the $CuFeS_2$ chalcopyrite has been considered as a potential *n*-type material for thermoelectric application [1–5]. The thermoelectric efficiency of a material defined by its figure of merit ZT is equal to $\alpha^2T/\rho(\kappa_{el}+\kappa_{lat})$, where *T* is the absolute temperature, α the Seebeck coefficient, ρ the electrical resistivity, κ_{el} the electronic contribution to the thermal conductivity and κ_{lat} the thermal conductivity of the lattice (phonons) [6,7]. ZT can also be deduced from the power factor, $PF = \alpha^2/\rho$, by the relation: $ZT = PF*T/(\kappa_{el}+\kappa_{lat})$. In that respect, the high PF value reported for doped $CuFeS_2$ [1–5] makes this material attractive, especially if one considers that it is made of cheap and abundant elements as compared to other recently reported semiconductors crystallizing also in the chalcopyrite structure [8–10]. In addition, $CuFeS_2$ is an antiferromagnet ($T_N = 823$ K) [11], and it was proposed that the spins could play a role on the transport properties [2]. Also, there exists a structural transition close to T_N from the tetragonal space group of the chalcopyrite to a cubic zinc blende structure above T_N in which the Cu and Fe cations are disordered over the tetrahedral crystallographic sites [12].

This situation motivated us to study the effect of carrier doping by substituting a magnetic cation to optimize its thermoelectric properties. In the same time, the *p*-type counterpart $CuFeSe_2$ has also been synthesized and its transport properties measured. Also $CuFeS_2$ and $CuFeSe_2$ have similar 1:1:2 atomic contents, they crystallize in different structures [13]. The latters can be described by a tetragonal close-packed

* Corresponding author. Laboratoire CRISMAT, UMR 6508 ENSICAEN/CNRS, ENSICAEN, UCBN, 6 boulevard du Maréchal Juin, 14050 Caen Cedex 4, France.
E-mail address: antoine.maignan@ensicaen.fr (A. Maignan).
Peer review under responsibility of The Chinese Ceramic Society.

http://dx.doi.org/10.1016/j.jmat.2015.03.007

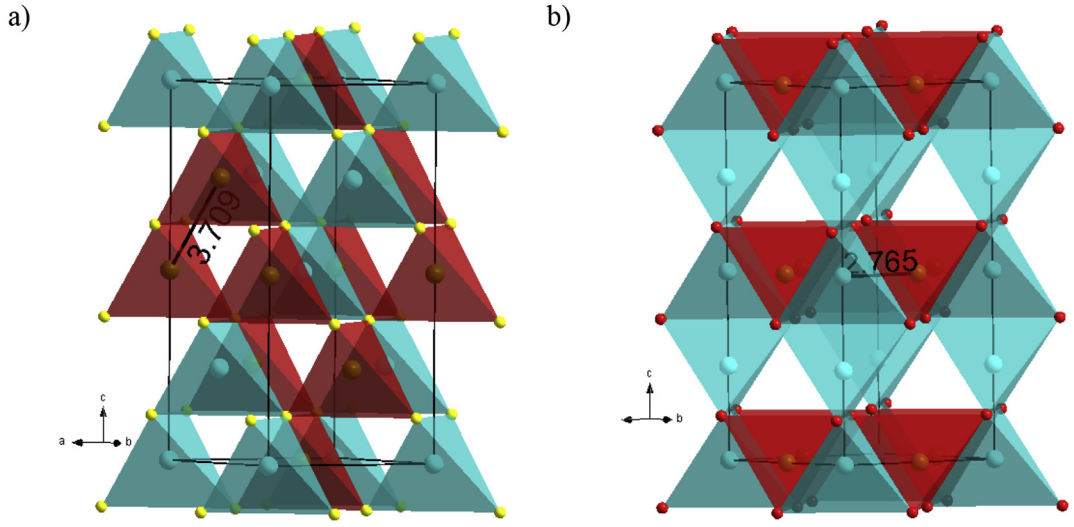

Fig. 1. Views of the crystals structures of (a) $CuFeS_2$ and (b) $CuFeSe_2$. Shortest metal–metal distances are shown for both structures.

stacking of S^{2-} or Se^{2-} anions in which the Cu and Fe cations are distributed differently over the empty tetrahedral sites (Fig. 1). As a consequence, even if the sulfur coordination of Cu and Fe is tetrahedral, the metal–metal distance shrinks by almost 1 Å as one goes from $CuFeS_2$ or $CuFeSe_2$. This is believed to explain the semimetallic character of $CuFeSe_2$ as compared to the semiconducting behavior of $CuFeS_2$. For the latter, it must be pointed out that it can be classified as a "Haldane-Anderson" type insulator with a strong d-p hybridization, 80% of the holes of Fe^{3+} in the formally written $Cu^{+}Fe^{3+}$ S_2^{2-} formula being transferred on sulfur anions [14].

In the following, the properties of $CuFeSe_2$ and $CuFeS_2$ are compared and the effect of Co doping in $CuFeS_2$ is studied. A ZT value reaching ZT = 0.22 at 675 K is achieved for $Cu_{0.94}Co_{0.06}FeS_2$.

2. Experimental

The $Cu_{1-x}Co_xFeS_2$ and $CuFeSe_2$ polycrystalline samples were first prepared by mixing Cu, Fe, Co and S/Se in the appropriate ratio. After sealing the cold pressed powder in a close ampoule, the latter was heated at 600 °C for 48 h. For some compositions, the obtained powder was then sintered by SPS using a maximum temperature of 500 °C for 30 min under a pressure of 70 Mpa, followed by cooling in 20 min. The density of these SPS pucks was found to be greater than 90%. The crystallographic quality was determined by using powder X-ray diffraction data. Rietveld refinement of the highly densified sample was performed with the FULLPROF program using pseudo-Voigt peak shape function. Transmission Electron Microscopy (TEM) measurements, including high resolution TEM (HRTEM) and electron diffraction (ED) studies, were performed using Tecnai G2 30 UT (LaB_6) microscope operated at 300 kV and having 0.17 nm point resolution. This microscope is equipped with a EDAX detector for EDX analysis. TEM specimens made of powders were prepared by crushing the samples in agate mortar, dissolving in methanol and depositing on Ni holey carbon grid. Transport option of a physical properties measurement system (PPMS from Quantum Design) was also used to measure the electrical resistivity (ρ) and a home-made puck was used to measure the Seebeck coefficient (S), (steady-state technique) up to 300 K in the same cryostat. For T > 300 K, a Ulvac Riko ZEM3 system working under a helium partial pressure was used to measure ρ and S. The thermal conductivity κ was obtained for T > 300 K by combining thermal diffusivity and heat capacity data measured with Netzsch systems operating in N_2 flow.

3. Results

3.1. Structural characterizations

The room temperature powder X-ray diffraction patterns (Fig. 2) of $CuFeSe_2$ and $Cu_{1-x}Co_xFeS_2$ evidence first the

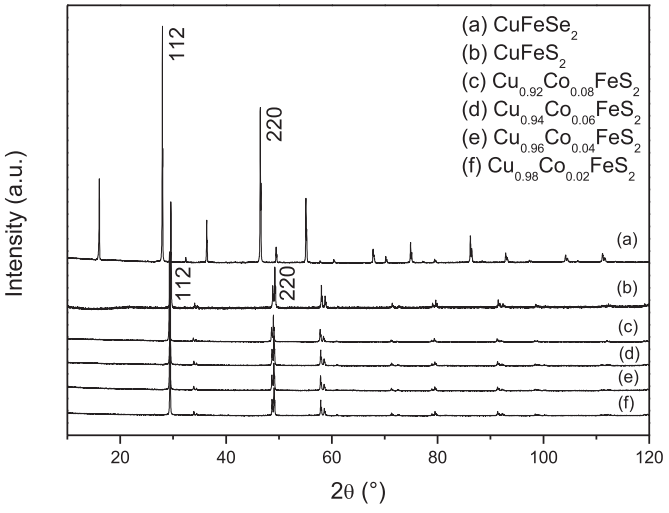

Fig. 2. Powder diffraction patterns of $CuFeCh_2$ samples obtained after solid state reaction. *hkl* index are given for the main peaks of both structure type.

structural difference between the eskebornite (*P-42c* space group) and chalcopyrite (*I-42d*). No extra peaks could be hardly observed for both $CuFeSe_2$ and $CuFeS_2$ (Fig. 2a) and b)). For $Cu_{1-x}Co_xFeS_2$ by varying x by 0.02 from $x = 0.00$ to 0.20, it turns out that impurities (mainly CoS_2) were detected from $x = 0.10$. For that reason, the study was limited to $x \leq 0.08$. Also, as the $Fe_{1-x}Co_xS_2$ solid solution with the pyrite structure exists [15], even if Fe or Co divalent cations are in octahedral coordination in that structure, attempts to substitute Co for Fe in $CuFeS_2$ were made. However, extra peaks were always detected even for the lowest content corresponding to the nominal "$CuFe_{0.98}Co_{0.02}S_2$" formula. This indicates that the divalent oxidation state of cobalt being more stable in sulfides, Co^{2+} cannot substitute easily Fe^{3+} in "$Cu^{+}Fe^{3+}S_2^{2-}$", but, rather, it substitutes for monovalent copper as it was previously shown for other substituting elements as Zn^{2+} in $Cu_{1-x}Zn_xFeS_2$ or for the series $Cu_{1-x}Fe_{1+x}S_2$ [2–5]. According to the limited solubility of Co for Cu (8% at maximum) determined from X-ray diffraction by detection of secondary phases, it must be also pointed out that all our attempts to make copper deficient $Cu_{1-x}FeS_2$ compounds led to the formation of impurities from the powder X-ray diffraction pattern. In order to confirm the veracity of the Co for Cu substitution, electron diffraction studies, performed with a transmission electron microscope coupled to EDX, and HRTEM imaging were all made for the $x = 0.06$ "SPS" sample (Fig. 3). The local composition analysis using EDX, in the accuracy of the techniques,

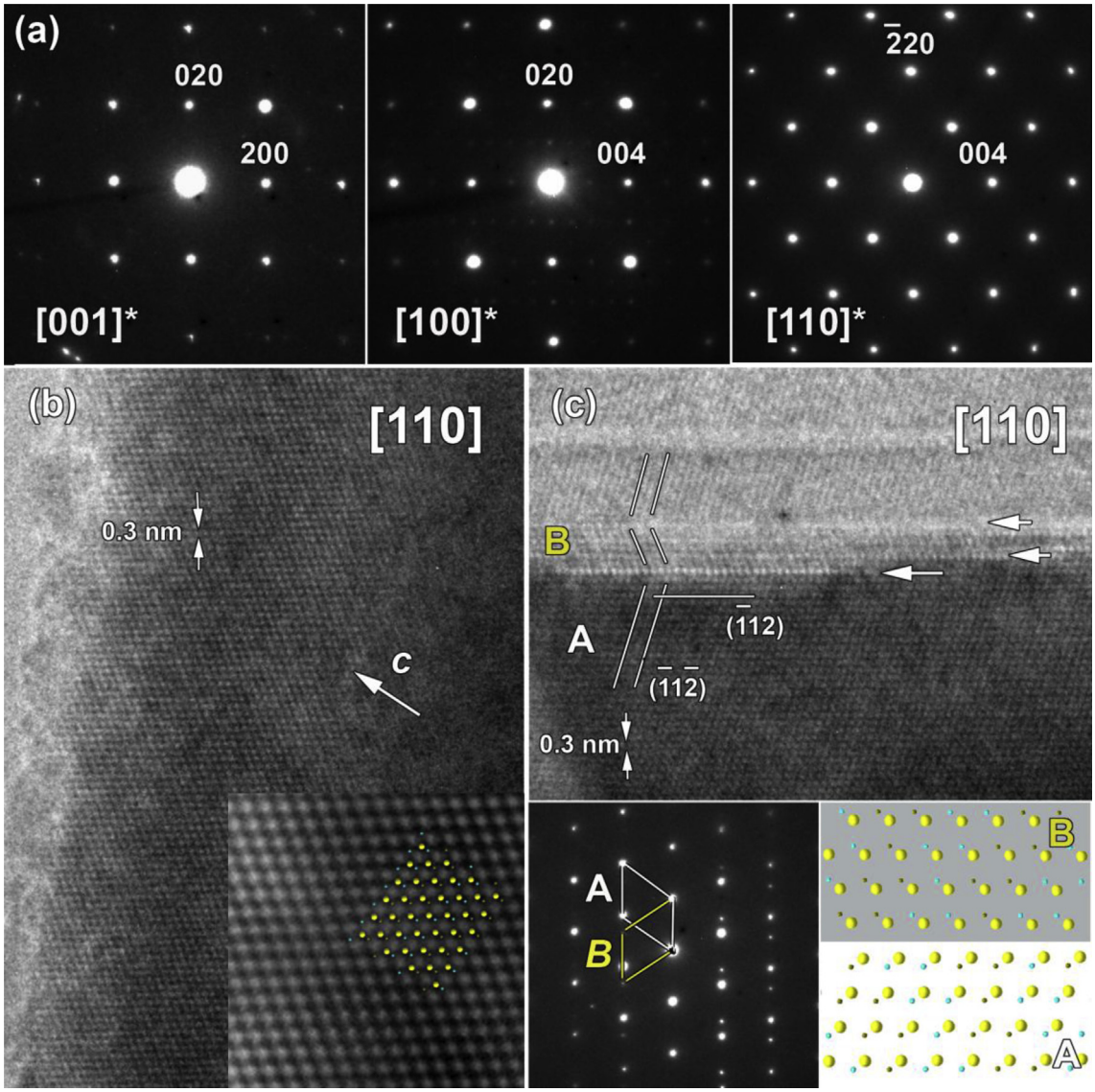

Fig. 3. (a) ED patterns of "SPS" $Cu_{0.94}Co_{0.06}FeS_2$ from main zone axis: [001]*, [100]* and [110]* (b) HRTEM image of $Cu_{0.94}Co_{0.06}FeS_2$ along [110] zone axis with an overlay model given as insert (blue −Cu/Co, green − Fe, yellow − S). Note that under present image conditions, the bright dots correspond to the voids and the dark ones to the atoms position. (c) [110] HRTEM image of twinned area and corresponding ED pattern. Twinning planes are marked by white arrows. A structural model of the twin boundary is given as insert (right bottom corner) where two twin variants are marked as A and B, correspondingly.

performed on several tenths of microcrystallites confirms that cobalt is definitely present within each crystallites of $Cu_{1-x}Co_xFeS_2$ with an estimated cation composition: 0.94 ± 0.02:0.06 ± 0.02:1:00 ± 0.02 in good correspondence with the cation content in the nominal $Cu_{0.94}Co_{0.06}FeS_2$ formula. The ED patterns collected from main zone axis shown in Fig. 3a can be indexed based on tetragonal *I-42d* structure (*SG 122, a = 0.53 nm, c = 1.042 nm)* of $CuFeS_2$ [16]. The ED patterns and corresponding HRTEM images (Fig. 3b) show that the compound is well crystallized. A comparison of the experimental and calculated HRTEM images (not shown here) shows, that under present experimental conditions, the columns of atoms are imaged as the darkest regions. Twinning was the only kind of defects which was observed. The HRTEM image and corresponding ED pattern of a twinned area are shown in Fig. 3c. The ED pattern is the superposition of two $Cu_{1-x}Co_xFeS_2$ slices (marked in the figure as A and B) and exhibits splitting of diffraction spots which is typical of twinned structure. From the ED pattern, the twinning plane is {112}. The twin slices are limited by sharp coherent twin boundaries parallel to the (−112) plane. The rows of the bright dots (marked by white arrowheads) indicate the twin boundaries. The dot brightness is higher than that of the matrix suggesting different atomic arrangement along twin boundaries. From the crystallographic viewpoint, such twinning is often observed in cubic phases. As the present material exhibits a transition from the *I-42d* tetragonal structure at room temperature to an *F-43m* cubic structure at high temperature (~800 K, [12]), i.e. such a kind of twinning is consistent with the fact that its RT structure is close to cubic. Such local antiphase domains of small size might also play a role in the phonon scattering as it was invoked for the "TAGS" thermoelectric materials [17].

3.2. Physical properties

3.2.1. $CuFeSe_2$ and $CuFeS_2$: evidence for very different groundstates

The measurements of electrical resistivity (ρ) and Seebeck coefficient (S) evidence the very different groundstates for the sulfide and selenide (Fig. 4(a)). $CuFeSe_2$ exhibits a semi-metallic character with $\rho_{300K} = 0.35$ Ω.cm which is consistent with the already reported data of the literature [13]. Its S(T) curve is linear with S > 0 values, indicating the *p*-type nature of the transport as expected for a metal-like behavior. S increases with T up to $S \approx +15$ μV.K^{-1} at 300 K, which remains a modest value. This metallic like behavior is in marked contrast with the semiconducting behavior of $CuFeS_2$ which S(T) values are negative, indicating a *n*-type behavior, and which absolute values, $S_{300K} \approx -350$ μV.K^{-1}, are much larger than those of $CuFeSe_2$. It must be emphasized that the concomitant decrease of both electrical conductivity and Seebeck coefficient as temperature decreases supports a behavior near the intrinsic one as discussed in Ref. [5]. These ρ and S values lead to very different values for the power factor, PF(275 K) = 1.10^{-5} W.K^{-2}.m^{-1} and 5.10^{-8} W.K^{-2}.m^{-1} for $CuFeS_2$ and $CuFeSe_2$, respectively (Fig. 4(b)). Thus, the

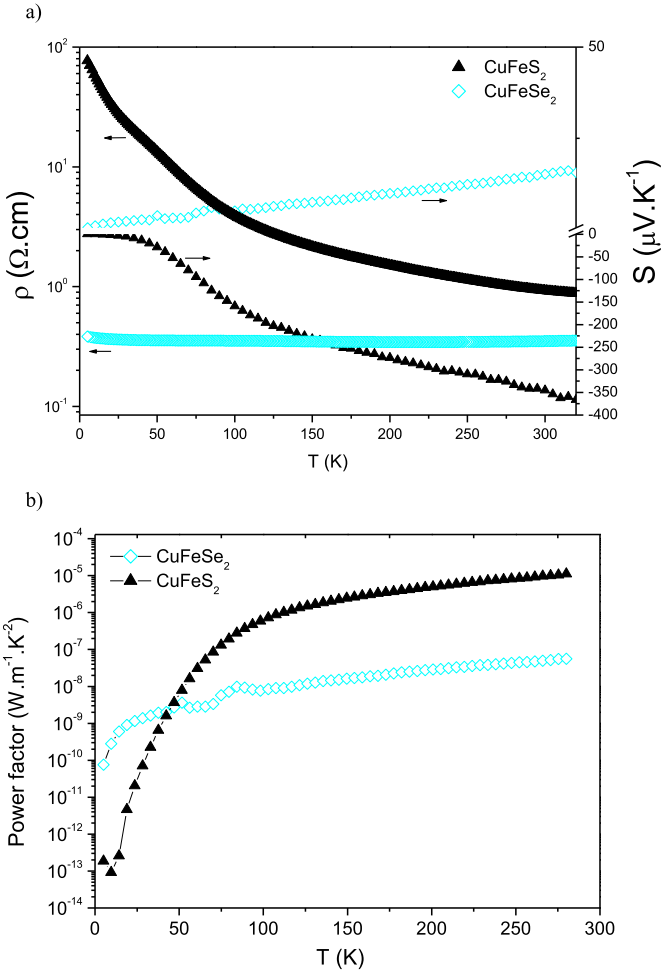

Fig. 4. (a) Temperature (*T*) dependence of the electrical resistivity (ρ), left y-axis and Seebeck coefficient (S), right *y*-axis of $CuFeSe_2$ and $CuFeS_2$ measured at low temperature (b) T dependence of the power factor of $CuFeSe_2$ and $CuFeS_2$ measured at low *T*.

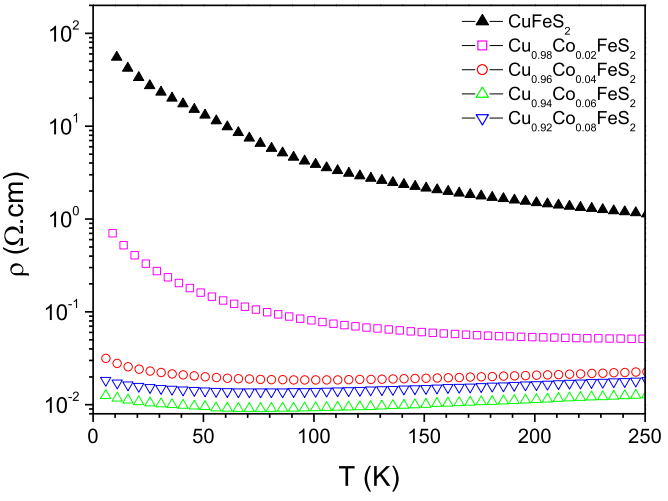

Fig. 5. *T* dependence of *ρ* measured at low temperature on samples prepared by solid state reaction and cold pressed.

metallic behavior of $CuFeSe_2$, which might be linked to the metal bonding created by short intermetallic distances in the eskebornite structure, is redhibitory for the use of $CuFeSe_2$ as a thermoelectric material. This motivated the study of Co doping in the $CuFeS_2$ chalcopyrite only.

3.2.2. $Cu_{1-x}Co_xFeS_2$

At first, low temperature measurements have been carried out on cold pressed samples, and the corresponding ρ(T) curves are plotted in Fig. 5. As compared to $CuFeS_2$, the cobalt substitution for copper induces a decrease of electrical resistivity, to reach a metallic behavior over a broad range of temperature for $x \geq 0.04$. The resistivity of Co-doped samples decreases with the increase of cobalt amount from $Cu_{0.98}Co_{0.02}FeS_2$ to $Cu_{0.94}Co_{0.06}FeS_2$. For the $x = 0.08$ sample, the resistivity keeps similar values as for $Cu_{0.94}Co_{0.06}FeS_2$, which suggests a limit of Co substitution close to 6% in good agreement with the solubility limit determined by powder X-ray diffraction. This ρ decrease with the increase of the Co amount suggests the creation of charge carriers resulting from a Co^{2+} for Cu^{+} aliovalent substitution.

The low temperature dependence of S (Fig. 6) confirms that scenario. All the $Cu_{1-x}Co_xFeS_2$ samples show a *n*-type behavior with absolute value of Seebeck coefficients that decrease with x increasing. The lack of linear SαT regime is consistent with a behavior of degenerate semiconductor. The corresponding PF values obtained from these measurements are shown in Fig. 7. The highest PF values at 275 K are obtained for the $Cu_{0.96}Co_{0.04}FeS_2$ and $Cu_{0.94}Co_{0.06}FeS_2$ samples, with $PF = 1.75.10^{-4}$ $W.K^{-2}.m^{-1}$ and $PF = 2.25.10^{-4}$ $W.K^{-2}.m^{-1}$, respectively. Therefore samples of both compositions were densified by SPS to estimate their thermoelectric performances.

The high temperature dependence of S (Fig. 8) for these "SPS" samples exhibits an increase of the absolute value of S with T, reaching at 675 K maximal values of 240 μV/K and 275 μV/K for $Cu_{0.94}Co_{0.06}FeS_2$ and $Cu_{0.96}Co_{0.04}FeS_2$, respectively. It must be pointed out that the S (275 K) values are in good correspondence with those collected on cold pressed samples (Figs. 6 and 8). This supports the fact that the overall stoichiometry is preserved during the SPS process, so that no S deficiency as for the $CuFeS_{2-x}$ series [1] is created.

The corresponding ρ(T) curves are plotted in Fig. 8 (left y-scale) for the same T range. For both samples densified by SPS, the curves confirm a metallic behavior with ρ increasing with T up to ~600 K. Above ~600 K, ρ starts to saturate and then to decrease in the case of $Cu_{0.94}Co_{0.06}FeS_2$ (Fig. 8). This might be ascribed to the beginning of the structural transition which is complete at ~800 K [12]. Interestingly, the densification by SPS induces a decrease of the electrical resistivity: for $Cu_{0.94}Co_{0.06}FeS_2$ at 275 K, $\rho \approx 5.4.10^{-3}$ Ω.cm for the SPS prepared dense sample against $\rho \approx 1.3.10^{-2}$ Ω.cm for the cold pressed one (Fig. 4). Consequently, as S is kept unchanged and

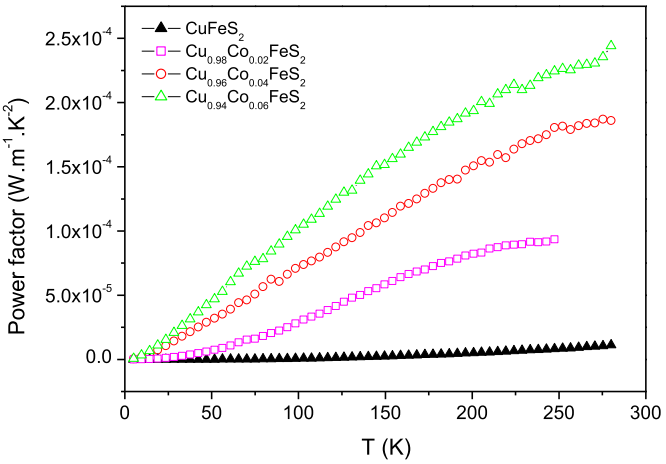

Fig. 7. *T* of the power factor measured at low *T* on samples prepared by solid state reaction and cold pressed.

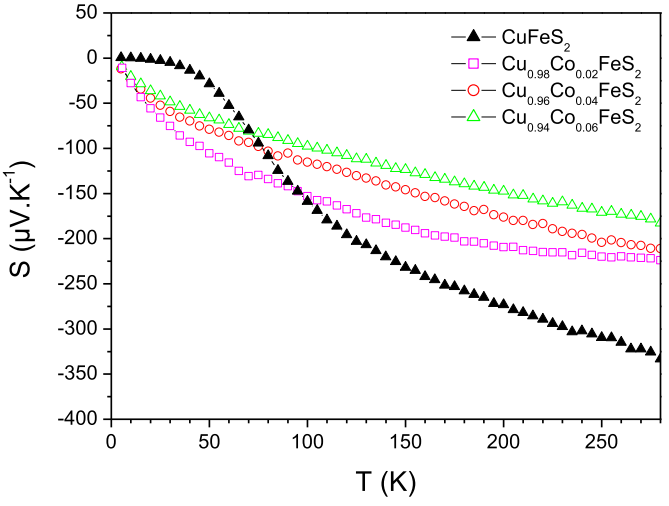

Fig. 6. *T* dependence of S measured at low temperature on samples prepared by solid state reaction and cold pressed.

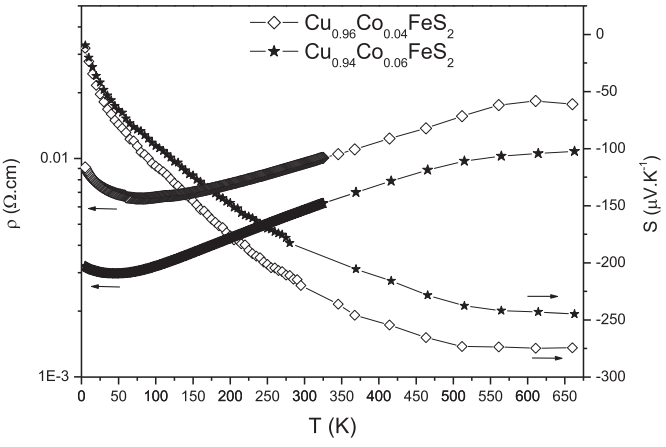

Fig. 8. *T* dependence of both S and *ρ* at high *T* for both samples densified by SPS, $Cu_{0.96}Co_{0.04}FeS_2$ and $Cu_{0.94}Co_{0.06}FeS_2$.

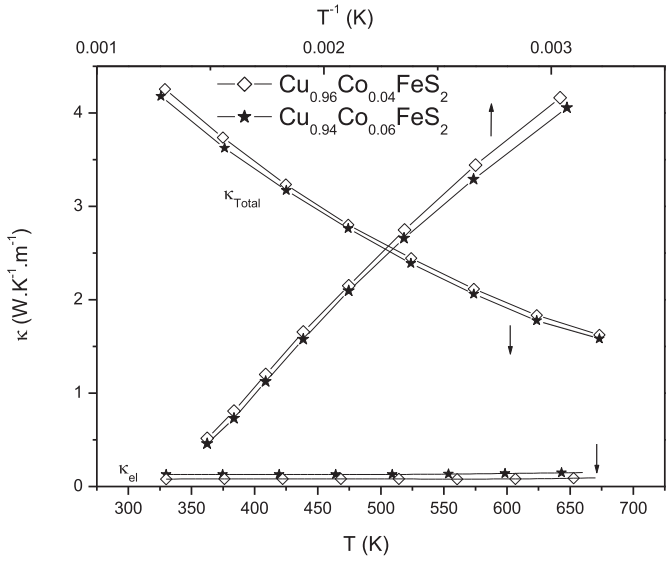

Fig. 9. T and T^{-1} dependence of the thermal conductivity κ at high T for $Cu_{0.96}Co_{0.04}FeS_2$ and $Cu_{0.94}Co_{0.06}FeS_2$ densified by SPS.

ρ decreases, the PF values are enhanced to reach maximum values of PF ≈ $5.5.10^{-4}$ $W.m^{-1}.K^{-2}$ and PF ≈ $6.2.10^{-4}$ $W.m^{-1}.K^{-2}$ at 370 K for $Cu_{0.94}Co_{0.04}FeS_2$ and $Cu_{0.94}Co_{0.06}FeS_2$, respectively.

The thermal conductivities κ as a function of T for these SPS prepared samples are presented in Fig. 9. The κ value decreases as T increasing, to reach values as low as $\kappa_{600K} \approx 2$ $W.K^{-1}.m^{-1}$. When plotted in the form $\kappa(T^{-1})$, linear behaviors are observed up to 600 K. They are characteristic of phonon dominated thermal conductivities. This is also consistent with the very low κ_{el} values, calculated from the Wiedemann-Franz law (See corresponding curves in Fig. 9), which represent less than 10% of the total thermal conductivity over the whole temperature range.

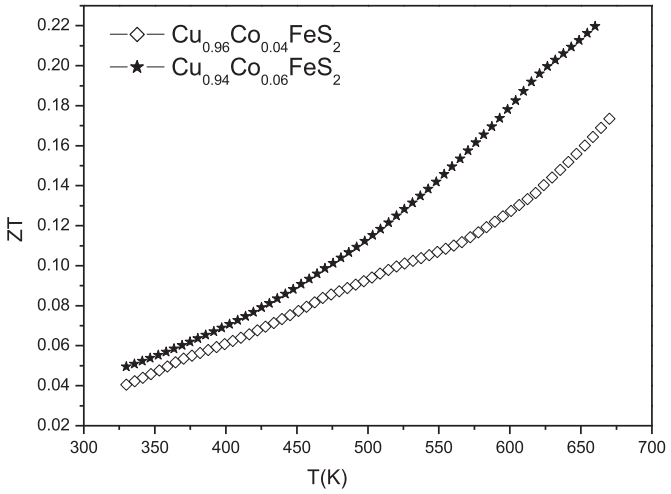

Fig. 10. T dependence of the figure of merit ZT for $Cu_{0.96}Co_{0.04}FeS_2$ and $Cu_{0.94}Co_{0.06}FeS_2$ densified by SPS.

Combining PF and κ, the corresponding values of the dimensionless figures of merit ZT were calculated (Fig. 10). At 675 K, a highest ZT value of 0.22 is achieved for $Cu_{0.94}Co_{0.06}FeS_2$.

4. Discussion and concluding remarks

The present κ values, very similar for $Cu_{0.96}Co_{0.04}FeS_2$ and $Cu_{0.94}Co_{0.06}FeS_2$, with $\kappa_{400K} \approx 3.5$ $W.K^{-1}.m^{-1}$, are smaller than the values reported in Ref. [4] for $Cu_{0.97}Zn_{0.03}FeS_2$ (x = 0.03 and 0.05) which were all around 5–6 $W.K^{-1}.m^{-1}$ at 400 K. At 575 K, for the present $Cu_{1-x}Co_xFeS_2$ samples, they are close to the values given in Ref. [1] for sulfur deficient $CuFeS_{2-x}$ with x ≈ 0.15. Such a similarity for the κ values of the present Co-substituted $CuFeS_2$ dense samples with the best values observed for S deficient $CuFeS_2$ samples demonstrates the efficiency of the Co substitution for Cu to reduce the lattice part of the thermal conductivity. The very close values of κ for the x = 0.04 and x = 0.06 compounds are consistent with the fact that the lattice contribution is dominating.

The role of cobalt could result from its magnetic character as compared to zinc in $Cu_{1-x}Zn_xFeS_2$. More work would be needed to demonstrate a change in the magnetic properties. Finally, the best ZT value, 0.22 at 675 K is equivalent to the highest ZT values reported for materials derived from $CuFeS_2$, the highest value having been reported for a S-deficient compound, $CuFeS_{1.80}$, with ZT = 0.21 at 573 K [1]. The present results suggest that by combining Co for Cu substitution and S deficiency, even highest ZT values should be reached.

Acknowledgments

The authors gratefully thank G. Renouf and F. Veillon for technical assistance.

References

[1] Li J, Tan Q, Li J-F. Synthesis and property evaluation of $CuFeS_{2-x}$ as earth-abundant and environmentally-friendly thermoelectric materials. J Alloys Compd 2013;551:143–9.
[2] Tsujii N. Possible enhancement of thermoelectric properties by use of a magnetic semiconductor: carrier-doped chalcopyrite Cu_{1-x} Fe_{1+x} S_2. J Electron. Mater 2013;42:1974.
[3] Tsujii N, Mori T. High thermoelectric power factor in a carrier-doped magnetic semiconductor $CuFeS_2$. Appl Phys Express 2013;6:043001.
[4] Tsujii N, Mori T, Isoda Y. Phase stability and thermoelectric properties of $CuFeS_2$-based magnetic semiconductor. J Electron Mater 2014;43:6.
[5] Li Y, Zhang T, Quin Y, Day T, Snyder GJ, Shi X, et al. Thermoelectric transport properties of diamond-like $Cu_{1-x}Fe_{1+x}S_2$ tetrahedral compounds. J Appl Phys 2014;116:203705.
[6] Heikes RR, Ure Jr RW. Thermoelectricity: science and engineering. New York, London: Interscience Publishers; 1961.
[7] Rowe DM. CRC handbook of thermoelectrics. In: Rowe DM, editor. Boca Raton, FL: CRC Press; 1995.

[8] Liu R, Xi L, Liu H, Shi X, Zhang W, Chen L. Ternary compound $CuInTe_2$: a promising thermoelectric material with diamond-like structure. Chem Commun 2012;48:3818.
[9] Yusufu A, Kurosaki K, Kosuga A, Sugahara T, Ohishi Y, Muta H, et al. Thermoelectric properties of $Ag_{1-x}GaTe_2$ with chalcopyrite structure. Appl Phys Lett 2011;99:061902.
[10] Kosuga A, Plirdpring T, Higashine R, Matsuzawa M, Kurosaki K, Yamanaka S. High-temperature thermoelectric properties of $Cu_{1-x}InTe_2$ with a chalcopyrite structure. Appl Phys Lett 2012;100:042108.
[11] Donnay G, Corliss LM, Donnay JDH, Elliot N, Hastings J. Symmetry of magnetic structures: magnetic structure of chalcopyrite. Phys Rev 1958;112:1917.
[12] Engin TE, Powell AV, Hull S. A high temperature diffraction-resistance study of chalcopyrite, $CuFeS_2$. J Solid State Chem 2011;184:2272.
[13] Lamazares J, Jaimes E, D'onofrio L, Gonzalez-Jimenez F, Sanchez Porras G, Tovar R, et al. Magnetic susceptibility, transport and Mössbauer measurements in $CuFeSe_2$. Hyperfine Interact 1991;67:1–4. 517-521.
[14] Sato K, Harada Y, Taguchi M, Shin S, Fujimori A. Characterization of Fe 3*d* states in $CuFeS_2$ by resonant X-ray emission spectroscopy. Phys Status Solidi A 2009;206(5):1096–100.
[15] Guo S, Young DP, Macaluso RT, Browne DA, Henderson NL, Chan JY, et al. Charge transport in cobalt-doped iron pyrite. Phys Rev B 2010;81:144424.
[16] Hall SR, Stewart JM. The crystal structure refinement of chalcopyrite $CuFeS_2$. Acta Crystallog B 1973;29:579–85.
[17] Cook BA, Kramer MJ, Wei X, Harringa JL, Levin EM. Nature of the cubic to rhombohedral structural transformation in $(AgSbTe_2)_{15}(GeTe)_{85}$ thermoelectric material. J Appl Phys 2007;101:053715.

Dr. Antoine Maignan, is a CNRS Research Director, Director of the CRISMAT Laboratory. He received his PhD in Sciences in 1988. The CRISMAT laboratory is famous for its discoveries of new transition metal oxides with properties such as high Tc cuprates, CMR manganites, and thermoelectric cobaltites. The research of Antoine Maignan consists in the investigation of strongly correlated systems, showing multiferroics or thermoelectric properties. He has published 591 papers and 54 proceedings (H index = 62). He has given 110 invited talks at international conferences. Antoine Maignan is President of the « European Thermoelectric Society » since 2011.

Dr. Berthebaud, is a CNRS researcher at the CRISMAT laboratory, Caen, France. He received the Phd degree in chemistry in 2007 from University of Rennes, France. He then was a post-doctoral researcher at CBPF laboratory in Rio de Janeiro, Brasil, in 2008 before joining the National Institute for Materials Science in Tsukuba, Japan, until 2010. Before joining CRISMAT in 2011, he worked at University of Montpellier, France. His research activities focus on solid state chemistry of intermetallics and chalcogenides, including thermoelectric materials. He has published over 20 papers based on his research.